Article

Hydrogen Cycling of Niobium and Vanadium Catalyzed Nanostructured Magnesium

H. Gijs Schimmel, Jacques Huot, Laurent C. Chapon, Frans D. Tichelaar, and Fokko M. Mulder

J. Am. Chem. Soc., **2005**, 127 (41), 14348-14354• DOI: 10.1021/ja051508a • Publication Date (Web): 27 September 2005

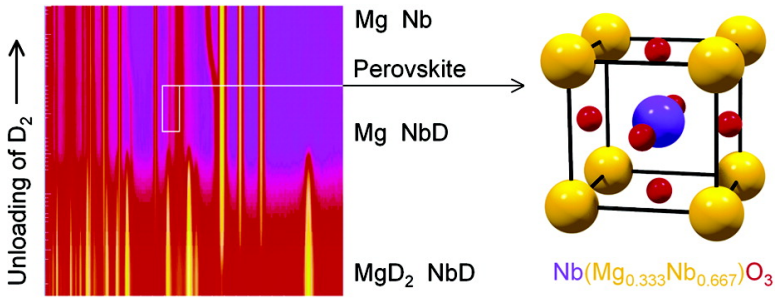

More About This Article

Additional resources and features associated with this article are available within the HTML version:

- Supporting Information
- Links to the 8 articles that cite this article, as of the time of this article download
- Access to high resolution figures
- Links to articles and content related to this article
- Copyright permission to reproduce figures and/or text from this article

View the Full Text HTML

J|A|C|S
ARTICLES
Published on Web 09/27/2005

Hydrogen Cycling of Niobium and Vanadium Catalyzed Nanostructured Magnesium

H. Gijs Schimmel,[†] Jacques Huot,[‡] Laurent C. Chapon,[§] Frans D. Tichelaar,[||] and Fokko M. Mulder*,[†]

Contribution from the Department of Radiation, Radionuclides and Reactors, Faculty of Applied Sciences, Delft University of Technology, Mekelweg 15, 2629JB Delft, The Netherlands, the Institut de recherche sur l'hydrogène, Université du Québec à Trois-Rivières, (Qc)G9A 5H7 Canada, the ISIS facility, Rutherford Appleton Laboratory, Chilton, Didcot, United Kingdom, and the National Centre for HREM, Delft University of Technology, The Netherlands

Received March 9, 2005; E-mail: f.m.mulder@tnw.tudelft.nl

Abstract: The reaction of hydrogen gas with magnesium metal, which is important for hydrogen storage purposes, is enhanced significantly by the addition of catalysts such as Nb and V and by using nanostructured powders. In situ neutron diffraction on $MgNb_{0.05}$ and $MgV_{0.05}$ powders give a detailed insight on the magnesium and catalyst phases that exist during the various stages of hydrogen cycling. During the early stage of hydriding (and deuteriding), a $MgH_{1<x<2}$ phase is observed, which does not occur in bulk MgH_2 and, thus, appears characteristic for the small particles. The abundant H vacancies will cause this phase to have a much larger hydrogen diffusion coefficient, partly explaining the enhanced kinetics of nanostructured magnesium. It is shown that under relevant experimental conditions, the niobium catalyst is present as NbH_1. Second, a hitherto unknown Mg−Nb perovskite phase could be identified that has to result from mechanical alloying of Nb and the MgO layer of the particles. Vanadium is not visible in the diffraction patterns, but electron micrographs show that the V particle size becomes very small, 2−20 nm. Nanostructuring and catalyzing the Mg enhance the adsorption speed that much that now temperature variations effectively limit the absorption speed and not, as for bulk, the slow kinetics through bulk MgH_2 layers.

1. Introduction

A *conditio sine qua non* for the development of sustainable technologies for the hydrogen economy is the availability of an economical, safe, and practical hydrogen storage mechanism. Since hydrogen gas can be used as a clean fuel both in conventional combustion engines and in fuel cells, it has a large potential as an energy carrier. Hydrogen is a very light and volatile gas, which forces the use of low temperatures, high pressures, a sorption material, or a combination of these to store a practical amount of hydrogen (6 wt % in the year 2010 according to the demand of the Department of Energy of the USA). Magnesium metal stores approximately 7.6 wt % in the form of MgH_2, which is a transparent insulator. Its use is at present hampered by the slow kinetics, which makes it practical only at temperatures above 300 °C.[1] By means of a ball milling treatment the particle size can be reduced, which speeds the sorption properties by a factor of 10. The addition of a catalyst like V or Nb increases the kinetics by another order of magnitude.[1−3] Because niobium and vanadium do not alloy with Mg nor form intermetallic compounds, these will be heterogeneously catalyzed materials.

1.1. Kinetic Factors in the Reaction of Hydrogen and Magnesium. Magnesium metal transforms into magnesium hydride in a gas−solid reaction. The driving force for this process scales with $\ln(P_{applied}/P_{equilibrium})$. The hydriding reaction of metallic magnesium involves several steps: (1) gas permeation through the particle bed, (2) surface adsorption and hydrogen dissociation, (3) migration of hydrogen atoms from the surface into the bulk, (4) diffusion through the particle and finally (5) nucleation and growth of the hydride phase.[4,5] In principle each of these steps might be rate-limiting, and many reports are known that study one or more of these steps.[6−14]

[†] Department of Radiation, Radionuclides and Reactors, Delft University of Technology.
[‡] Université du Québec à Trois-Rivières.
[§] Rutherford Appleton Laboratory.
[||] National Centre for HREM, Delft University of Technology.

(1) Huot, J.; Liang, G.; Schulz, R. *Appl. Phys. A* **2001**, *72*, 187.
(2) Zaluski, L.; Zaluska, A.; Ström-Olsen, J. O. *J. Alloys Compd.* **1997**, *253*−*254*, 70.
(3) Huot, J.; Liang, G.; Boily, S.; Neste, A. V.; Schulz, R. *J. Alloys Compd.* **1999**, *293*−*295*, 495.
(4) Gérard, N.; Ono, S. In *Hydrogen in Intermetallic Compounds II*; Schlapbach, L., Ed.; Springer: 1992.
(5) Sastri, M. C. V.; Viswanathan, B.; Murthy, S. S. *Metal Hydrides*; Springer-Verlag: Berlin, 1998.
(6) Liang, G.; Huot, J.; Boily, S.; Schulz, R. *J. Alloys Compd.* **2000**, *305*, 239.
(7) Zaluska, A.; Zaluski, L.; Ström-Olsen, J. O. *J. Alloys Compd.* **1999**, *289*, 197.
(8) Bloch, J.; Mintz, M. H. *J. Alloys Compd.* **1997**, *253*−*254*, 529.
(9) Martin, M.; Gommel, C.; Borkhart, C.; Fromm, E. *J. Alloys Compd.* **1996**, *238*, 193.
(10) Rudman, P. S. *J. Appl. Phys.* **1979**, *50*, 7195.
(11) Luz, Z.; Genossar, J.; Rudman, P. S. *J. Less-Common Met.* **1980**, *73*, 113.
(12) Belkbir, L.; Joly, E.; Gerard, N. *Int. J. Hydrogen Energy* **1981**, *6*, 285.

10.1021/ja051508a CCC: $30.25

Regarding the first step, this is more of an engineering problem, and we will therefore not discuss it here. The second step is rate-limiting in magnesium since the addition of catalysts for this process increases the kinetics drastically.[1] The kinetics of the third step will, like the second step, scale with the surface area of the particles. Previously we have shown using ab initio computer calculations that the diffusion of hydrogen through magnesium *metal* is not rate-limiting at practical temperatures and particles sizes around 1 μm, even though the concentration of hydrogen in the metal phase is very low.[15] The nucleation and growth process, finally, will lead to considerable interfacial energy because magnesium metal has a completely different crystal structure than magnesium hydride. To overcome such a barrier, excess pressure for the creation of nucleation centers is needed. In this respect it is not unlikely that some hydrogen saturated catalyst particles in close contact with a Mg particle act as nucleation centers as well.

On decreasing the particle size by ball milling magnesium hydride, a high density of defects and distortions is introduced. Previously, we have shown that the abundant defects and distortions in the magnesium hydride structure play no decisive role in the increase of the sorption speed as they are annealed out when the hydrogen content is cycled, while the kinetics remain fast.[16,17] We will therefore regard the ball milling treatment mainly as a method to produce nanostructured and catalyzed magnesium particles in large quantities.

The main contributions to the increase in speed when the particles are nanostructured are therefore sought in the increase of the specific surface area, the decrease of diffusion path lengths, and factors concerning nucleation and growth in nano particles. Next, Nb and V catalysts are known for their catalytic activity in the reaction of hydrogen with Mg. Mg does not form alloys or intermetallic compounds with Nb or V.[18] Thus when preparing Nb catalyzed Mg samples, one does not expect to alloy Mg and Nb. The questions where the catalyst atoms are and in which phase are important for a more detailed understanding of the mechanism behind the catalytic activity. In this contribution a time-dependent, in situ neutron diffraction study on the hydriding and dehydriding properties of ball milled and catalyzed $MgNb_{0.05}H_2$ and $MgV_{0.05}H_2$ is presented. In previous work the Nb phase has been observed using X-ray diffraction,[19,20] and a solid solution gateway phase of H in Nb was proposed. In contrast to the X-ray experiments, the use of neutrons enabled us to locate hydrogen in the structures and refine hydrogen site occupancies during hydrogen loading and unloading of the samples. This makes an improved understanding of the nanostructured Mg−Nb−H and Mg−V−H systems possible.

2. Experimental Section

Magnesium hydride powder and niobium or vanadium metal powder were ball-milled in a Spex 8000 ball milling apparatus for 20 h. Under an inert atmosphere, respectively 2.15 g of the $MgNb_{0.05}H_2$ and 2.11 g of the $MgV_{0.05}H_2$ sample was loaded in quartz tubes that were connected to a gas-handling system. After heating to 320 °C hydrogen gas was first released from the cell while maintaining the equilibrium pressure, with a controlled constant hydrogen flow, and diffraction spectra were taken during desorption. Deuterium was then loaded as this isotope provides a different contrast in neutron diffraction experiments. Successive release of deuterium and finally the loading of hydrogen completed the experiment. Diffraction patterns were collected during all these stages using the GEM diffractometer at the ISIS facility. At the temperatures of our experiment, no structural differences between the hydride and deuteride form of the catalyst exist, at least in bulk form. The hydrogen containing samples produce a huge background due to the large incoherent cross section of hydrogen, but nevertheless GEM provides a remarkably good signal-to-noise ratio sufficient for detailed Rietveld analysis showing that these patterns yield the same results as those of the deuterides.

The loading of deuterium or hydrogen gas was performed at a temperature that was regulated to be 320 °C within 1 °C and mostly at a pressure around 4−5 bar, finishing at 11 bar, much higher than the equilibrium pressure of 2.5 bar at this temperature. A neutron diffraction pattern was recorded for each of the loading steps (20 for the niobium sample, 11 for the vanadium sample) in the loading process. From a calibrated volume at room temperature and the pressure drop in it, the amount of deuterium or hydrogen that was absorbed in the magnesium sample was determined. During unloading, also at a constant temperature of 320 °C, deuterium or hydrogen was released at a constant desorption rate of 5 mL/min (STP conditions; 1 bar, rt), and pressures were recorded. A diffraction pattern was acquired every 3 min, and a total of 83 patterns for the niobium sample and 87 patterns for the vanadium sample were taken.

GEM is a high intensity, good resolution neutron diffractometer at the ISIS facility of the Rutherford Appleton Laboratory in the United Kingdom.[23] The 7290 neutron detectors are grouped into 7 banks, each with a different range of accessible *d*-spacing. GEM combines an unprecedented neutron count rate with a very large *Q* range and good resolution, facilitating detailed in situ measurements. The data were corrected for the contribution from the empty quartz sample container. All patterns of the complete cycles were sequentially fitted using the Rietveld refinement program GSAS.[24] The phase fractions, lattice parameters, hydrogen site occupancies, and line widths were allowed to vary freely. The patterns of the different detector banks were fitted simultaneously.

High-resolution electron microscopy photographs and selected area diffraction patterns were obtained using a 300 kV Philips CM300UT-FEG machine. Quantitative elemental composition was studied by energy dispersive spectroscopy. Samples were prepared by ultrasonic shaking of the powder in ethanol and drying it on a copper grid with a holey carbon foil. Separate powder particles were examined with diffraction, imaging, and EDS (Energy Dispersive Spectroscopy) for elemental analysis.

3. Experimental Results and Analysis

The patterns obtained during dehydriding of the Mg−Nb sample are shown as a color plot in Figure 1 together with the

(13) B. Vigeholm, K.; Jensen, B. L.; Pedersen, A. S. *J. Less-Common Met.* **1987**, *131*, 133.
(14) Mintz, M. H.; Gavra, Z.; Hadari, Z. *J. Inorg. Nucl. Chem.* **1978**, *40*, 765.
(15) Schimmel, H. G.; Kearley, G. J.; Huot, J.; Mulder, F. *J. Alloys Compd.* **2004**, in press.
(16) Schimmel, H. G.; Johnson, M. R.; Kearley, G. J.; Ramirez-Cuesta, A. J.; Huot, J.; Mulder, F. M. *Mater. Sci. Eng. B* **2004**, *108*, 38.
(17) Schimmel, H. G.; Johnson, M. R.; Kearley, G. J.; Ramirez-Cuesta, A. J.; Huot, J.; Mulder, F. *J. Alloys Compd.*, accepted for publication.
(18) Massalski, T. B. *Binary alloy phase diagrams*, 2nd ed.; ASM International: Metals Park, 1990; Vol. 3.
(19) Pelletier, J. F.; Huot, J.; Sutton, M.; Schulz, R.; Sandy, A. R.; Lurio, L. B.; Mochrie, S. G. J. *Phys. Rev. B* **2001**, *63*, 052103.
(20) Yavari, A. R.; de Castro, J. F. R.; Vaughan, G.; Heunen, G. *J. Alloys Compd.* **2003**, *353*, 246.
(21) Flanagan, T. B.; Oates, W. A. In *Hydrogen in Intermetallic Compounds II*; Schlapbach, L., Ed.; Springer: 1992.
(22) F. D. Manchester, Ed. *Phase diagrams of binary hydrogen alloys*; ASM International: Materials Park, 2000.
(23) Williams, W. G.; Ibberson, R. M.; Day, P.; Enderby, J. *Physica B* **1998**, *241−243*, 234.
(24) Larson, A. C.; Dreele, R. B. V. *General Structure Analysis System (GSAS)*, LAUR 86-748; Los Alamos National Laboratory: 1994.

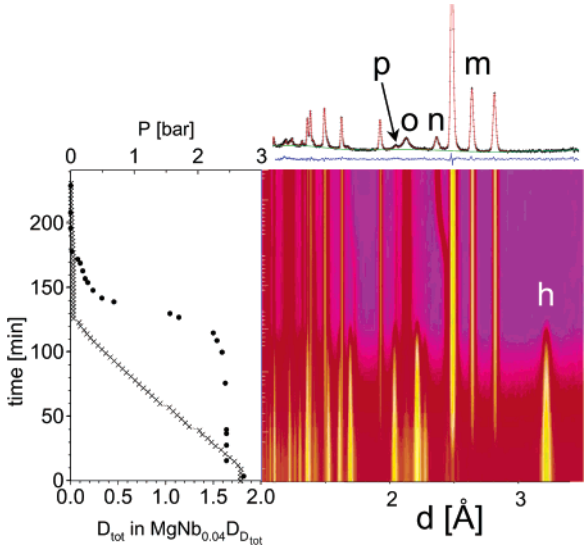

Figure 1. Image of neutron diffraction patterns during the desorption of deuterium, plotted against desorption time. Against the same time axis also the fitted integral content D_{tot} of deuterium is given (×) as well as the gas pressure (●). The horizontal axis to the right shows a fraction of the *d*-spacing range measured. Reflections from the five different phases are indicated: Mg (m), MgD_2 (h), MgO (o), Nb (n), and the perovskite phase (p).

hydride fraction and the pressure as a function of time. Five phases could be identified in the patterns: Mg metal, MgH_2, MgO, α-NbD_x and a small, but clearly visible and identifiable contribution from a perovskite phase that we discuss below. The data of the Mg−V sample was analyzed in the same way and produced equivalent results for the Mg, MgH_2, and MgO phases. However, no sign of vanadium in metallic, deuteride, hydride, or other form was found. One of the reasons for this may be that V has a very low coherent neutron cross section. Below, we will discuss the electron microscopy measurements that we performed to detect the vanadium. First we present the findings for the niobium catalyzed sample from the neutron scattering experiment.

3.1. Neutron Scattering Results. From the fits we obtained the phase fractions, lattice parameters, site occupancies, temperature factors, and line widths. The line widths are determined by the effective particle size and the strain in the particles. In these experiments, no significant changes in the line widths of the phases were found. Detailed results were obtained for the deuterides as well as the hydrides of the Nb and V catalyzed materials. Because the samples show identical results concerning the Mg, $Mg(H/D)_2$, and MgO, for the sake of brevity only the $MgNb_{0.05}D_2$ sample is described in detail, and where necessary remarks are made concerning the other samples. For the Mg−Nb compound, the phase fractions, hydrogen occupancies, and lattice parameters of the different phases are plotted as a function of the effective composition $MgNb_{0.05}D_{D_{tot}}$ in Figure 2.

The results for the site occupation of the magnesium deuteride phase when its concentration is low is remarkable. We see that (i) the site occupancy *y* of deuterium in MgD_{2y} can be as low as about $y = 0.5$, much lower than its stoichiometric value $y = 1$ in the bulk, and (ii) this affects the lattice parameters of the unit cell. Above an effective sample composition $D_{tot} = 0.3$, the structural parameters of the magnesium deuteride phase converge to the usual values, which remain constant from then on. In the analysis it was also considered to have a separate $MgD_{2y<2}$ phase for loadings higher than $D_{tot} = 0.3$ next to a stoichiometric MgD_2 phase, but this appeared not to be necessary for a good fit. Nevertheless it appears likely that individual Mg particles start with deuteriding (hydriding) with such substoichiometric composition. The same hydrogen deficient $MgH_{2y<2}$ phase is observed in the protonated sample. The incoherent cross section of deuterium for neutrons contributes significantly to the background level; therefore a decrease of the background level during deuterium extraction is observed in Figure 1.

During the deuteration (or hydriding) process (triangles in Figure 2) the volume of the unit cell of magnesium (hexagonal space-group $P6_3/mmc$) starts to increase by about 0.05 $Å^3$ per unit cell. The deuterium entering the magnesium metal phase will increase the volume of the unit cell due to the extra volume of the hydrogen atom which is generally assumed to be 2−3 $Å^3$ per hydrogen atom.[25] From the assessment of the Mg−H system by Zeng et al. we derive a concentration of hydrogen in magnesium metal of about 10^{-3} under our experimental conditions.[15,26] However, the lattice expansion that we observe is much larger than expected from the composition $MgH_{0.001}$ and therefore has to be attributed mainly to temperature effects induced by the energy released during hydrogen absorption. This occurs inside the bulky sample, notwithstanding the fact that the temperature regulation was constant within ±1 K. The linear thermal expansion coefficient of magnesium metal at these temperatures is 30×10^{-6}/K. This means that the volumetric expansion is about 90×10^{-6}/K, from which it is derived that the temperature of the magnesium metal has to increase by about 12 K to show this effect. The peak in the unit cell volume at a loading of 0.2 may indicate that initially the temperature rise is quite high as the heater circuit has to adapt to the situation in which heat is generated inside the sample. The other phases in the system show a similar and consistent dependence of the unit cell volume upon hydrogen cycling.

The diffraction peaks of the α-Nb phase can be fitted consistently in all of the patterns. The fits indicate that Nb is present in an effective composition of approximately NbD during the loading and unloading of Mg. In the last stage, when all MgD_2 has been converted into Mg, the pressure becomes lower than the equilibrium pressure of NbD (about 0.1 bar for this phase at this temperature), which then converts to Nb metal by lowering the D content gradually. The lattice of NbD_x shrinks when its deuterium content *x* is reduced, which is clearly visible in the s-shapes around $d = 2.4$ and 1.7 Å in the upper part of the color plot. When NbD_x releases its deuterium, the MgD_2 has vanished already completely. This means that for the actual catalytic hydrogen splitting into atoms one should consider NbD to be the more relevant phase.

At room temperature bulk niobium metal possesses an α-phase which contains hydrogen up to a concentration of $NbH_{0.25}$. It is a metallic hydride which possesses the typical α−α′ transition such as that present in other metallic hydrides such as palladium.[21] In analogy to a gas-to-liquid transition a critical point is present at 171 °C.[22] Under our experimental conditions the niobium particles are above their critical point and the α-phase may contain hydrogen in the composition NbH_x, with $0 < x < 1$, depending on the pressure.

(25) Fukai, Y. *Z. Phys. Chem.* **1989**, *164*, 165.
(26) Zeng, K.; Klassen, T.; Oelerich, W.; Bormann, R. *Int. J. Hydrogen Energy* **1999**, *24*, 989.

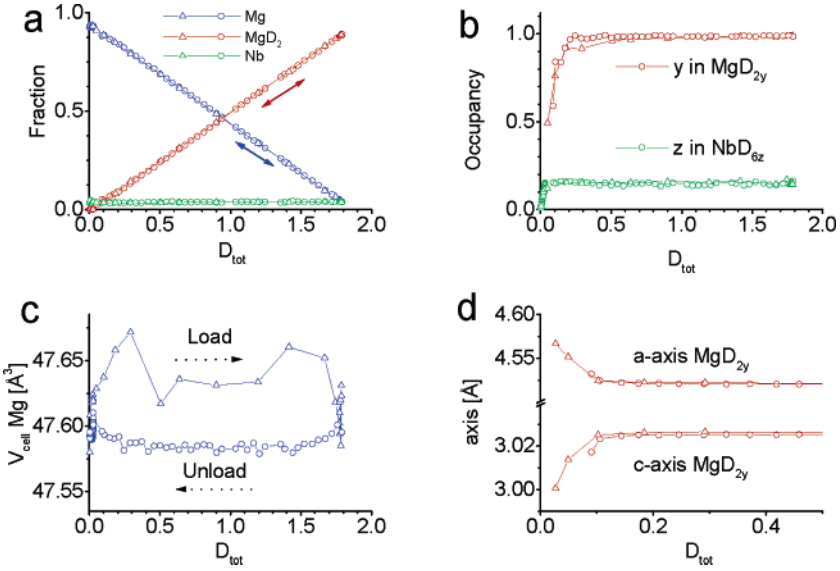

Figure 2. Structural parameters of Mg (blue), MgD_2 (red), and Nb (green) during loading (△) and unloading (○) of hydrogen as a function of D_{tot}, the hydrogen content: (a) phase fractions of Mg, MgD_2, and Nb; (b) site occupancies y of D in MgD_{2y} and z of D in NbD_{6z}; (c) unit cell volume of Mg; and (d) lengths of the a- and c-axes of the unit cell of MgD_{2y}.

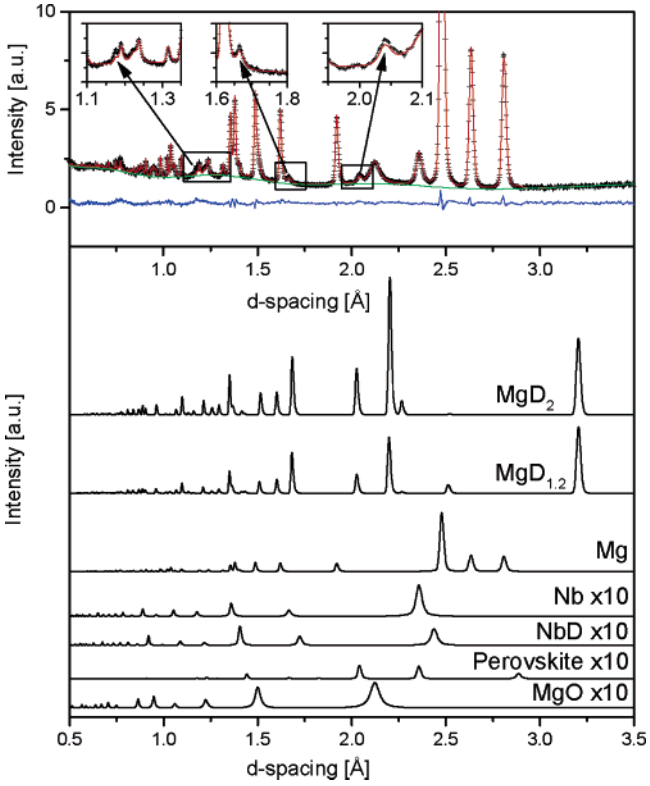

Figure 3. Rietveld refinement of the fully dehydrided sample. Three unique peaks that belong to the perovskite phase are indicated by the arrows in the insets. Below: simulated patterns of the subspectra identified in the Nb catalyzed Mg−H system, with, from top to bottom, MgD_2, $MgD_{1.2}$, Mg, Nb, NbD, $Nb(Mg_{0.333}Nb_{0.667})O_3$, and MgO using the parameters from the fits.

A careful observation of the patterns shows that peaks are present that do not belong to one of the expected phases. Three peaks are identifiable by eye: at 2.035, 1.661, and 1.175 Å as shown in Figure 3. These are reflections at 4.07 Å divided by 2, $\sqrt{6}$ and $\sqrt{12}$, which points toward a cubic phase. We found that known perovskites such as $Pb(Mg_{0.333}Nb_{0.667})O_3$,[27,28] $SrNbO_3$,[29] and $BaNbO_3$[30,31] all possess a cubic perovskite structure with lattice parameters around 4.05 Å at room temperature. Other cubic phases such as cubic NbO and MgO all have lattice parameters that are clearly larger (close to 4.21 Å) than what is observed here. We therefore propose that during the ball-milling process part of the Nb has been alloyed with the outer oxide layers of the Mg particles, leading to materials with the composition like $Nb(Mg_{0.333}Nb_{0.667})O_3$. Because the peaks are best visible in the fully dehydrided patterns, we first analyzed these patterns carefully to be able to characterize this new phase in more detail. Subsequently all patterns were refined with the amount of this perovskite phase as free variable. The refinements improved when this phase was added: for a single spectrum Chi-square reduced from 2.23 to 2.10. Notably, the fitted phase fraction appeared constant for all patterns during (de-)sorption, which shows the stability of the fitted contribution during large changes of the overall spectrum. Setting the molar amount of Mg to 100%, the sample contains 4% of Nb metal, 0.3% of $Nb(Mg_{0.333}Nb_{0.667})O_3$, and 7% of MgO, which leads to a bulk stoichiometry $Mg-Nb_{0.04}-O_{0.08}$. We present the data that were obtained for this phase in Table 1.

Figure 3 also gives the subpatterns of the individual phases that occur in the measurements. Note that different D site occupations in NbD_x and MgD_x have a relatively large influence on the peak intensities of the respective phases. Because of the very high counting rate of GEM these intensities are determined very accurately. The perovskite phase has only a small number of peaks of which several are visible by eye.

The case of V-catalyzed Mg is analogous to the Nb-catalyzed material with regards to the Mg, $Mg(H/D)_2$, and MgO phase. Though pure V metal is not visible in this particular experiment because of the extremely low coherent cross section of

(27) de Mattan, N.; Husson, E.; Gaucher, P.; Morell, A. *Mater. Res. Bul.* **1990**, *25*, 427.
(28) Bonneau, P.; Garnier, P.; Calvarin, G.; Husson, E.; Gavarri, J. R. *J. Solid State Chem.* **1991**, *92*, 350.
(29) Turzhevsky, S. A.; Novokov, D. L.; Gubanov, V. A.; Freeman, A. J. *Phys. Rev. B* **1994**, *50*, 3200.
(30) Casais, M. T.; Alonso, J. A.; Rasines, I.; Hidalgo, M. A. *Mater. Res. Bul.* **1995**, *30*, 201.
(31) Grin, Y.; Müller-Buschbaum, H.; von Schnering, H. G. *Z. Naturforsch., B: Chem. Sci.* **1997**, *52*, 153.

Table 1. Structural Parameters of the Phases Observed during Deuterium Cycling of Nb Catalyzed and Ball Milled MgD_2

	MgD_2
lattice parameter	$a,b = 4.530$ Å, $c = 3.025$ Å
space group	$P4_2/mnm$ no. 136 (tetragonal)
atom site in Wyckoff notation	Mg: 2a (0,0,0)
	D: 4f (0.3044(1),0.3044(1),0)
occupancy	Mg: 1.000(1)
	D: 1.000(1)
	$MgD_{1.2}$
lattice parameter	$a,b = 4.56$ Å, c=3.00 Å
space group	$P4_2/mnm$ no. 136 (tetragonal)
atom site in Wyckoff notation	Mg: 2a (0,0,0)
	D: 4f (0.3053(3),0.3053(3),0)
occupancy	Mg: 1.000(1)
	D: 0.60(5)
	Mg
lattice parameter	$a,b = 3.235$ Å, $c = 5.253$ Å
space group	$P6_3/mmc$ no. 194 (hexagonal)
atom site in Wyckoff notation	Mg: 2c (1/3,2/3,1/4)
occupancy	Mg: 1.000(1)
	Nb
lattice parameter	$a = 3.324$ Å
space group	$Im\bar{3}m$ No. 229 (body centered cubic)
atom site in Wyckoff notation	Nb: 2a (0,0,0)
occupancy	Nb: 1.000(1)
	NbD
lattice parameter	$a = 3.44$ Å
space group	$Im\bar{3}m$ no. 229 (solid solution bcc)
atom site in Wyckoff notation	Nb: 2a (0,0,0)
	D: 12d (1/4,0,1/2)
occupancy	Nb: 1.000(1)
	D: 0.16(2)
	$Nb(Mg_{0.333}Nb_{0.667})O_3$
lattice parameter	$a = 4.070$ Å
space group	$Pm\bar{3}m$ no. 221 (cubic perovskite)
atom site in Wyckoff notation	Nb: 1a (0,0,0)
	Nb,Mg: 1b (1/2,1/2,1/2)
	O: 3c (0,1/2,1/2)
occupancy	Nb: 1.0(1)
	Nb: 0.7(2), Mg: 0.3(2)
	O: 1.0(1)
	MgO
lattice parameter	$a = 4.227$ Å
space group	$Fm\bar{3}m$ no. 225 (cubic)
atom site in Wyckoff notation	Mg: 4a (0,0,0)
	O: 4b (1/2,1/2,1/2)
occupancy	Mg: 1.000(1)
	O: 1.000(1)

vanadium, VD or a V-perovskite similar to the one observed above could be visible because of the presence of good coherent scatterers such as D and O. However, the VD/H phase appears to be invisible, which may also be due to the fact that its strongest peak would overlap with the strongest MgO peak. Bulk vanadium hydride also possesses an $\alpha-\alpha'$ transition with a critical point at about 200 °C.[22] Therefore under the experimental conditions the hydrogen content of vanadium hydride particles is a continuous function of hydrogen pressure. Above 200 °C no phase transitions occur on hydrogen loading.[22] One may find compositions of VH_x in the range $0 < x < 2$, again depending on the hydrogen pressure.

3.2. Electron Microscopy Results for Mg−Nb and Mg−V. As stated above, we could not identify any vanadium in our series of diffraction patterns of the vanadium catalyzed sample. To clarify this situation, we performed additional measurements using transmission electron microscopy (TEM). Elemental analysis confirmed that V is indeed present in the sample and also in an amount that is consistent with the given sample composition $MgV_{0.05}$. Below we discuss the results of our TEM experiments on both the niobium and vanadium catalyzed sample.

In the Philips CM30UT-FEG TEM, separate powder particles were examined with diffraction, imaging, and EDS (Energy Dispersive Spectroscopy) for elemental analysis. Diffraction patterns from 1 μm^2 areas showed the presence of MgO and Mg clearly. In the electron microscopy graphs, shown in Figure 4, a typical result of the Nb sample is presented, where dark particles with sizes up to 50 nm can be identified, but particles of several hundred nanometers were also found. EDS on such particles confirmed the presence of Nb, and diffraction patterns consistent with metallic Nb were recorded.

Diffraction from powder particles in the V sample showed MgO lattice spacings clearly. In some powder particles, both MgO and Mg reflections were found. In this sample also dark particles were found but smaller (2−20 nm) than those in the Nb sample. Separate imaging of these particles turned out to be difficult since the cubic lattice structure and lattice parameter of metallic V (the phase of V as shown below) coincide with those of MgO within a few percent. Thus, lattice imaging does not distinguish between V and MgO with similar crystal size, neither does dark field imaging. Most successful was imaging without objective aperture in order to see absorption contrast of the heavier V particles in a powder particle. In this way about 10 particles were selected for local EDS, showing a clear V signal compared to no signal in the matrix surrounding such a particle. An example from the V sample is shown in Figure 5. Local diffraction on a particle showed a metallic cubic V phase. The neutron diffraction appears unable to observe the V and VD_x directly because of several reasons: the low coherent V cross section, small crystal size of the metallic V phase which causes line broadening in the measurements, and the position of the diffraction lines with respect to MgO.

4. Effect of Nanostructuring

The materials investigated here are nanostructured heterogeneous mixtures of Mg, $Mg(H/D)_2$, $Nb(H/D)_x$ or $V(H/D)_x$, and Mg containing oxides. The magnesium material undergoes a clear first-order phase transition upon (de-)intercalation with hydrogen or deuterium. There appears to be a remarkable and surprising influence of the nanostructuring on the phase transition and intercalation behavior, which to our knowledge was not observed before in hydrogen storage or more generally in intercalation compounds.

It is known that, for bulk micron sized particles, a shell of magnesium hydride is formed, which prevents the hydriding of the remaining metal core.[4,5] For the nanostructured materials the diffraction line widths indicate particle size in a range of 150 nm for the Mg and $Mg(H/D)_2$ phases. From the rather equal line widths of the Mg metal phase and the $Mg(H/D)_2$ phase, one deduces that there cannot be formed a closed shell of $Mg(H/D)_2$ around a Mg metal nucleus that blocks further hydriding of the Mg core; the observed deuteride/hydride phase particle size is too large for that compared to the grain size. This is unlike the situation in bulk Mg, and it gives a clear explanation why nanostructuring is advantageous. Because in stoichiometric MgH_2 H diffusion is very slow, the absence of such a closed shell removes an important kinetic bottleneck for application of Mg as storage material.

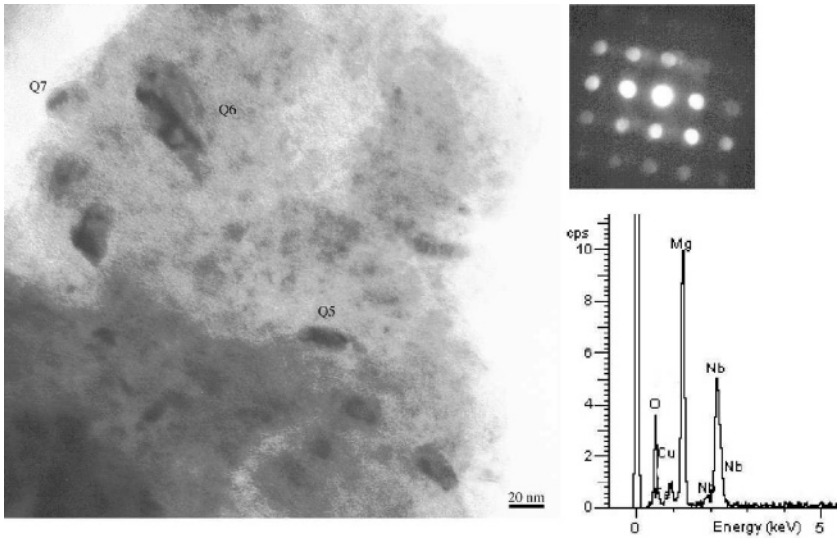

Figure 4. Bright field electron diffraction image showing several Nb particles. The diffraction pattern (taken with a convergent electron beam) shows 002 reflections with mutual 90° angles and distances to the origin that are consistent with the [001] beam direction in cubic Nb. The EDS shows a Nb line together with Mg and O signals from the surrounding material. The Cu signal is caused by the supporting grid.

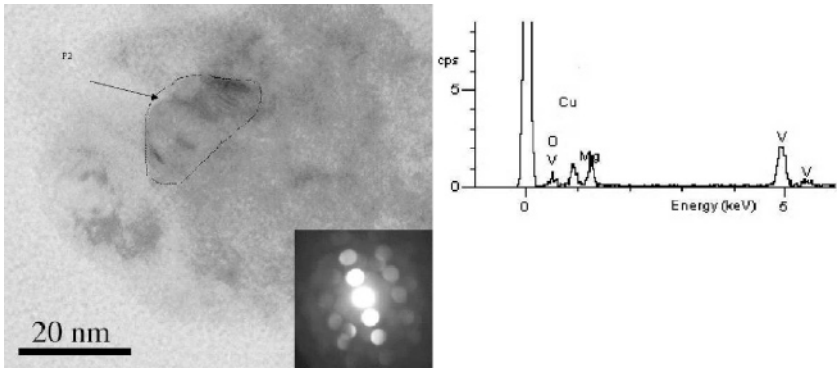

Figure 5. Absorption contrast image of part of a powder particle from the Mg−V sample. EDS shows the presence of V in particle P2. The Mg and O signals are caused by the surrounding matrix. The Cu signal is caused by the supporting grid. The diffraction pattern (taken with a convergent electron beam) shows 011 and 121 reflections with mutual angles and distances to the origin consistent with a [113] beam direction in the body centered cubic V phase. Some spurious reflections from the surrounding matrix are also visible.

Second, it appears that substoichiometric nanostructured $MgH_{x<<2}$ exists, which is impossible in bulk MgH_2. This is best observed in the first diffraction patterns of the hydrogen loading, where the hydride phase is becoming increasingly observable, and in the last patterns during unloading. The lower hydrogen occupancy is also reflected in altered unit cell dimensions. Such a hydrogen deficient phase likely exhibits a much faster diffusion of hydrogen due to the large concentration of vacancies, which will be a second factor in the enhancement of the hydrogen sorption speed for nanostructured Mg. After hydrogen and deuterium absorption cycles, these Mg particles remain smaller than a few hundered nanometers (on average 150 nm according to diffraction peak widths). The occurrence of substoichiometric $MgH_{x<2}$ may be considered a characteristic of nanocrystallinity.

The rationale for finding a hydrogen depleted MgH_2 phase may be as follows. In bulk particles the two-phase equilibrium leads to a limited amount of phase boundaries because the strains and mismatches between the two different lattices will be minimized. Nanostructured particles may not easily accommodate two phases with a (moving) boundary between them, because of the relatively large energy penalty of the induced strains. In such cases transition phases with intermediate compositions may be found, in contrast with the macroscopic phase diagram. Whether or not such intermediate composition occurs clearly depends on the difference in energy between such a phase and the stoichiometric phase, compared to the energy of the phase boundary. Since the area of the boundary, and therefore its energy, scales with the square of the particle size, whereas the energy difference between intermediate and stoichiometric phases scales with the cube of the particle size, there exists a certain particle size below which the intermediate composition phase appears energetically favorable. Altered intercalation behavior likely occurs more generally in nanostructured hydrogen and lithium intercalation materials and in more phenomena involving structural phase transitions.

Role of $Nb(H/D)_x$ and $V(H/D)_x$. The addition of Nb or V catalyzes both the desorption and the absorption process. In contrast to the X-ray experiments of Pelletier et al.[19] and Yavari et al.,[20] we did not find the $NbD_{0.6}$ or $NbH_{0.6}$ phase but rather higher D and H contents. We think that their finding is merely indicative that the pressure in the sample chamber is very low compared to our case during their desorption with high desorption rates. We find that during the complete Mg hydrogen cycling stage, $Nb(H/D)_{x\approx1}$ is present and only when the pressure is reduced below about 100 mbar the H or D content starts

lowering. The catalytic properties of NbH_1 rather than those of Nb metal are important for the desorption and the absorption process under real conditions, with pressures around 0.5−5 bar.

The Nb diffraction peak shape shows a particle size of about 42 nm. As for the role of V in catalyzing the reactions of hydrogen and magnesium metal, we found that vanadium breaks up in much smaller particles than niobium during the ball milling treatment. This means that more catalytic centers are available on the surface of the magnesium particles. This is thought to enhance the activity of vanadium with respect to niobium, which is supported by the finding that vanadium is the better catalyst.[1] Unfortunately, we could not extract any information about the phase that vanadium has in the ball milled samples from the neutron diffraction.

Nb(Nb,Mg)O_3 Perovskite a Possible Proton Conductor? A MgO phase is present on the surface of the Mg particles, even when the starting materials are always handled in an inert atmosphere. During (de-)sorption the MgO is a barrier for the transport of hydrogen. In this respect the small amount of the cubic Nb−Mg−O perovskite phase resulting from alloying of Nb and the MgO is an interesting finding. It is apparently present with particle sizes some two times larger than the average MgO particle size. Such perovskites are known to transport[32,33] and store[34] hydrogen and in addition may be catalysts themselves for splitting of H_2. The perovskite phase, penetrating the MgO layer, could therefore be the missing part of the hydrogen transport pathway.

The finding of such transition metal and Mg mixed oxide phases may be more general. Oxides such as Cr_2O_3, V_2O_5, Fe_3O_4,[35] and Nb_2O_5,[36] as well as some pure metals such as V and Nb,[37] are known to catalyze the hydrogen sorption properties of magnesium. Because all these transition metals T form compounds of the form $Mg_xT_yO_z$ (perovskite, spinel and other phases), it is interesting to investigate the catalytic activity of these compounds too. For instance $Mg_3V_xO_8$ are well-known catalysts used for hydrogenation reactions in the petrochemical industry.[38,39] Simulation of such a V containing material shows that the diffraction peaks strongly overlap with MgO.

Heat Effects. The observation of an increase in the unit cell volume of Mg during loading corresponds to a temperature rise of ∼12 K. The direct impact of this rise will be a higher equilibrium pressure, i.e., a reduction of the driving force for the growth of the hydride. Also the forming of new hydride nucleation centers inside the same particle becomes less probable. Both factors may play a role in the finding of a hydrogen depleted $MgH_{x<2}$, as well as in the absence of a closed MgH_2 shell around a Mg metal particle core (this should be formed by hydride nucleation centers on all sides of a Mg particle). We think that the heat that one growing nucleus generates prevents further nucleation especially for these small particle sizes. This means that only one nucleus may be formed, which cannot form a closed layer around a core.

The importance of heat effects for nucleation and growth may be estimated as follows. A particle contains N mol of magnesium atoms of which a fraction, f, has been converted to magnesium hydride. The heat that is released by the conversion to the hydride phase is $H_f = fH_{MgH2}N$, where H_{MgH2} is the formation enthalpy of magnesium hydride with respect to magnesium metal and hydrogen gas, 74.5 kJ/mol. The heat will increase the temperature of the magnesium particle by $\Delta T = H_f/(M_{Mg}C_{Mg}N)$, where we used the molar mass of magnesium $M_{Mg} = 0.0243$ kg/mol and the heat capacity $C_{Mg} = 1026$ J/(kg K). The equilibrium pressure becomes equal to the applied pressure (which we assumed to be 2 times the equilibrium pressure initially) when the temperature of the magnesium particle increases by about $\Delta T = 30$ K (for temperatures around 320 °C, for lower temperatures ΔT is lower). Knowing the parameters, $f = \Delta T M_{Mg}C_{Mg}/H_{MgH_2} = 1\%$ can be calculated. A fraction of 1% of a Mg particle transforming to MgH_2 generates sufficient heat to make the driving force zero due to the temperature rise of the particle. When this heat has been removed, clearly more hydrogen may absorb. A difference between a nanoscale particle and bulk will be that a relatively large fraction of the Mg in the nanoparticle is involved in a hydride nucleation center. Again this will make it more likely that only a single nucleation site is present in a nanoscale particle. In this way heat transfer is important not only for engineering sized batches but also for nucleation behavior at the particle level.

Conclusions

In situ neutron diffraction experiments reveal that nanostructured and Nb or V catalyzed Mg has characteristic properties explaining the enhanced sorption speeds. The occurrence of hydrogen depleted $MgH_{x<2}$ and the absence of a closed MgH_2 shell induced by a single $MgH_{x\leq 2}$ center in each particle may be considered as characteristic of the nanocrystallinity of the material. Unlike in bulk, heating of the material has now become the remaining limiting factor. Under conditions relevant for absorption and desorption, NbH was shown to be the relevant Nb hydride phase for the catalytic activity. In addition a new cubic perovskite phase with an estimated composition of Nb-$(Mg_{0.333}Nb_{0.667})O_3$ was indicated that may also be catalytically active as well as proton transporting. The V catalyzed material shows smaller V particle sizes than the Nb catalyzed material, but otherwise similar effects on the Mg phases are observed.

Acknowledgment. This work is a contribution from the Delft Center of Sustainable Energy (DCSE). Financial support was received from the Dutch Science Foundation (NWO) for access to ISIS. Special sample containers were provided by J. Dreyer and his team at ISIS.

Supporting Information Available: Crystallographic information files (CIF) are available for the Mg, MgD_2, $MgD_{1.2}$, MgO, Nb, NbD, and $Nb(Mg_{0.333}Nb_{0.667})O_3$ phases. This material is available free of charge via the Internet at http://pubs.acs.org.

JA051508A

(32) Goodenough, J. B. *Rep. Prog. Phys.* **2004**, *67*, 1915.
(33) Kreuer, K. D. *Annu. Rev. Mater. Res.* **2003**, *33*, 333.
(34) Mandal, T. K.; Sebastian, L.; Gopalakrishnan, J.; Abrams, L.; Goodenough, J. B. *Mater. Res. Bull.* **2004**, *39*, 2257.
(35) Oelerich, W.; Klassen, T.; Bormann, R. *J. Alloys Compd.* **2001**, *315*, 237.
(36) Barkhordarian, G.; Klassen, T.; Bormann, R. *J. Alloys Compd.* **2004**, *364*, 242.
(37) Liang, G.; Huot, J.; Boily, S.; Neste, A. V.; Schulz, R. *J. Alloys Compd.* **1999**, *291*, 295.
(38) Balderas-Tapia, L.; Wang, J. A.; Hernandez-Perez, I.; Aguilar-Rios, G. G.; Schacht, P. *Catal. Lett.* **2004**, *58*, 3034.
(39) Carrazán, S.; Peres, C.; Bernard, J.; Ruwet, M.; Ruiz, P.; Delmon, B. *J. Catal.* **1996**, *158*, 452.